IEEE Access
Multidisciplinary | Rapid Review | Open Access Journal

Received 25 October 2023, accepted 14 November 2023, date of publication 17 November 2023,
date of current version 29 November 2023.

Digital Object Identifier 10.1109/ACCESS.2023.3334264

RESEARCH ARTICLE

Tilted Circumnavigation of Multiple Drones Around Multiple Targets

MIRZOBEK MALIKOV, VLADIMIR SHIN, AND YOONSOO KIM, (Member, IEEE)
Graduate School of Mechanical and Aerospace Engineering, Gyeongsang National University, Jinju 52828, Republic of Korea

Corresponding author: Yoonsoo Kim (yoonsoo@gnu.ac.kr)

This work was supported by the National Research Foundation of Korea (NRF) funded by the Ministry of Science and ICT, Republic of Korea, under Grant NRF-2021R1A2C1004547.

ABSTRACT Existing strategies for coordinating a group of drones to follow a moving circular path while maintaining a specified distance between them (not necessarily identical) have generally involved circumnavigation around a single target or tracking an ellipse around multiple targets. The main drawback of tracking an ellipse is the difficulty of maintaining a constant velocity due to the variation in curvature around the ellipse. In this study, a novel strategy was developed so that drones track a tilted circle in the air whose projection becomes an ellipse on the ground that encloses multiple moving targets. By tracking a tilted circle, the drones can maintain an almost constant velocity while changing altitudes slightly with no inter-vehicle collision, which is technically much easier than tracking an ellipse directly in the air. To complete the tilted circumnavigation task, a vector-field guidance law followed by integral sliding-mode control was designed so that the following three conditions are satisfied under bounded disturbances: 1) all drones reach the plane of the tilted circle in the steady state; 2) each drone turns around the tilted circle's center with a time-varying radius in the steady state; and 3) drones avoid colliding with each other at all times. Numerical simulations showed that the proposed strategy was effective in situations mimicking real-life scenarios.

INDEX TERMS Circumnavigation, coverage ellipse, integral sliding model control (I-SMC), multiple target tracking, unmanned aerial vehicles (UAVs).

I. INTRODUCTION

A. MOTIVATION

The accelerating growth of unmanned aerial vehicles (UAVs) or drones has facilitated a wide range of inventive and pioneering applications in various fields. Drones that are equipped with high-resolution cameras and that are running computer vision algorithms in real-time have been attracting increased research attention [1], [2], [3]. In particular, small drones offer advantages such as flexible manipulation and improved endurance that enable them to handle complex tasks in cramped environments [4], [5], [6].

Among these complex tasks, a key task in the field of intelligent transportation is target tracking. Such targets may have both static and dynamic characteristics, which are normally known or estimated to enhance the tracking accuracy [7]. A group of drones can be used to accurately and reliably track moving ground targets [8], [9], and many strategies have been proposed for cooperative target tracking [10], [11], [12], [13], [14], [15], [16]. Several studies have explored using circular and elliptical orbits for drone navigation and target tracking. Li et al. [17] presented a cooperative circumnavigation strategy for UAVs to follow elliptical or circular orbits with varying radii in 3D space to track a single static or dynamic target. Similarly, Li et al. [18] proposed a control law to guide multiple microsatellites into a predefined elliptical orbit while maintaining a specific geometric formation around a host spacecraft. In practice, however, drones navigating around elliptical orbits is challenging because of the time-variant curvature of an ellipse. Moreover, drones require a high degree of control to follow an elliptical orbit, which can lead to inaccurate tracking.

In contrast, circular orbits are much easier for drones to follow while tracking multiple targets. Lawrence et al. [14]

The associate editor coordinating the review of this manuscript and approving it for publication was Nasim Ullah.

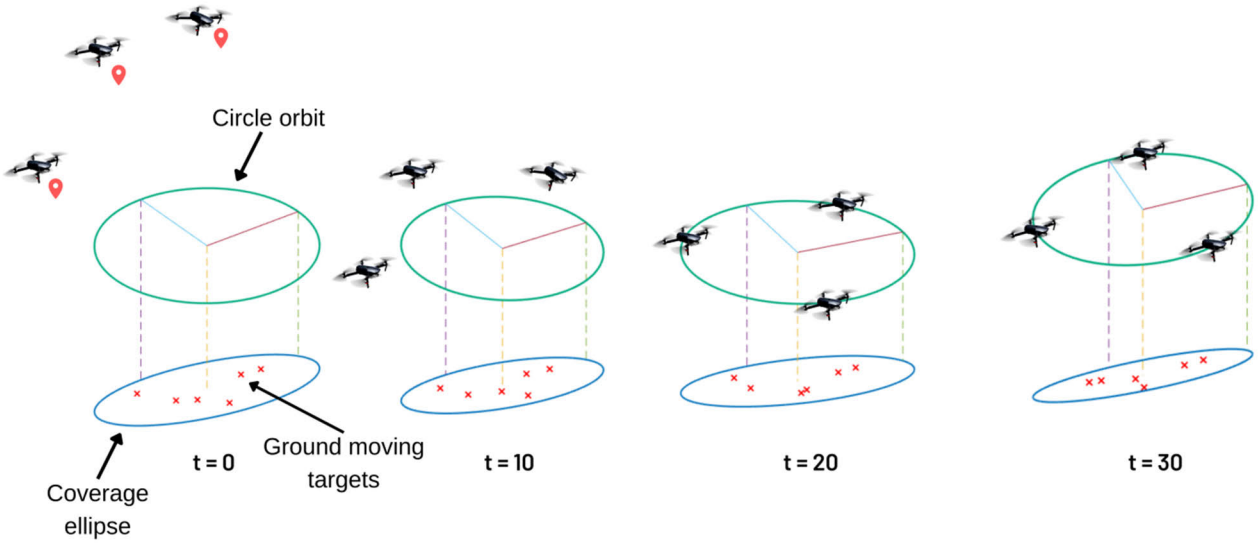

FIGURE 1. Motivation scenario: Three drones tilted circling six ground targets being located inside coverage ellipse at time instants 0, 10, 20 and 30 s.

generated a warped circular or racecar-like track for a group of drones spaced apart to loiter around fixed ground targets. Sun et al. [19] applied model predictive control to the circumnavigation of multiple UAVs and optimized their trajectories to join predetermined circular orbits. Park and Kim [12] proposed an interesting control strategy for a group of drones to track a single moving target and avoid collisions among themselves by following a circular orbit.

B. MAIN CONTRIBUTIONS

Park and Kim's [12] proposed cooperative collision-free target tracking strategy is for the circumnavigation of drones around a single moving target. However, tracking a single target uses a circular orbit whose radius and normal vector are constant, so this strategy cannot be directly applied to tracking multiple moving targets. The main theoretical difficulty lies in finding the best coverage area for targets in the absence of a command center that can collect information from all drones. In the present study, a distributed data processing approach was applied to identifying the best ellipse for enclosing all targets, which extends the previous circumnavigation strategy [12] to accommodate multiple moving targets and transforms the time-varying coverage ellipse into a circular orbit with a time-varying radius and normal vector.

The present study makes the following contributions:

1) A "tilted" circumnavigation strategy is proposed where drones follow a circular orbit angled rather than parallel to the ground for the effective and tight tracking of multiple targets.
2) To account for the limited viewing angle of a single drone, a probabilistic technique of distributed estimation is proposed so that multiple drones can work cooperatively to identify the smallest coverage ellipse of an arbitrary shape and the corresponding tilted circle via orthogonal projection to enclose multiple targets while considering measurement errors.
3) Vector-field guidance and integral sliding-mode control are applied to ensure that the proposed strategy works well in different scenarios even with disturbances.

   Numerical simulations were performed to demonstrate the efficacy of the proposed strategy in practical scenarios involving multiple targets and potential disturbances.

The rest of the paper is organized as follows. Section II formulates the study objective as three sub-problems. Section III introduces the distributed estimation technique used to identify the smallest ellipse enclosing multiple targets at each time instant and a transformation to obtain a tilted circle from the estimated coverage ellipse of an arbitrary shape. Section IV presents the proposed circumnavigation strategy. Section V presents the numerical simulations and their results. Section VI concludes the paper.

II. PROBLEM STATEMENT

Figure 1 shows the target scenario, where several drones are expected to track multiple targets on the ground. To track multiple targets rather than a single target, the drones should first calculate the smallest ellipse on the ground that encloses the targets and then calculate the corresponding tilted circle in the air. Because the targets are dynamic, the shape of the ellipse changes over time, which in turn means that the tilted circle has a time-varying center and radius. Once the tilted circle has been determined for a given time instant, guidance and control logics are activated to let the drones join and follow the tilted circle as they track the moving targets. In this paper, "tracking" is defined as the drones assuming positions immediately above the multiple targets. The

study objective can then be divided into the following three sub-problems:

1) Find or estimate the smallest ellipse that encloses all targets at each time step under the constraint that each drone has a limited viewing angle (i.e, one drone may not have full information on the locations of targets).
2) Derive a mathematical transformation between the smallest ellipse on the ground and a tilted circle in the air such that the projection of the tilted circle coincides with the ellipse.
3) Develop guidance and control laws such that drones at arbitrary initial positions join and follow the tilted circle while maintaining a prescribed inter-vehicle separation at all times to avoid collision.

III. SMALLEST ELLIPSE ENCLOSING TARGETS

In the present study, the distances between the drones and targets were assumed as known based on measurements taken by cameras mounted on the drones. These measurements can be employed in various approaches to calculate the smallest ellipse that encompasses the targets, of which several are described below.

A. DETERMINISTIC APPROACH

The deterministic approach involves finding the closed ellipse with the smallest area enclosing an $n-$ point set $(x_1, \ldots, x_n \in \mathbb{R}^2)$ in 2D space. The ellipse can be defined for $c \in \mathbb{R}^2$ and $Q \in \mathbb{R}^{2\times 2}$:

$$\mathcal{E}(c, Q) = \left\{x : (x-c)^T Q^{-1}(x-c) \leq 1\right\}, \tag{1}$$

where c is the center of the ellipse and the positive definite symmetric matrix $Q = Q^{\mathrm{T}} > 0$ determines its general shape. The area of $\mathcal{E}(c, Q)$ is given by $\pi[\det(Q)]^{1/2}$. Then the problem is equivalent to finding c and Q such that $[\det(Q)]^{1/2}$ is minimized subject to (1):

$$\begin{cases} \min\limits_{Q,c} [\det(Q)]^{1/2} \\ \text{s.t. } (x_i - c)^T Q^{-1}(x_i - c) \leq 1, \ i = 1, \ldots, n, \\ Q > 0. \end{cases} \tag{2}$$

By a change of variables [20], [21], $A = Q^{-1/2}$ and $b = Q^{-1/2}c$. Then, the optimization problem in (2) can be restated as

$$\begin{cases} \min\limits_{A,b} \left[-\log(\det(A))\right] \\ \text{s.t. } \|Ax_i - b\|_2 \leq 1, \ i = 1, \ldots, n, \\ A > 0. \end{cases} \tag{3}$$

Here, (3) is a convex optimization problem for A and b because $-\log(\det(A))$ is a strictly convex function in the space of positive definite symmetric matrices [20]. This problem can be easily solved by many methods [20], [21], [22]. If (A, b) is a solution to (3), then (2) can be solved by setting $(Q, c) = \left(A^{-2}, A^{-1}b\right)$.

TABLE 1. Parameters of coverage ellipse.

P_α	40%	63%	75%	90%	95%	97.5%	99%	99.5%
ℓ	1.0	2.0	2.77	4.61	5.99	7.38	9.21	10.6

B. CENTRALIZED STATISTICAL APPROACH

Although the deterministic approach is promising for finding the smallest coverage ellipse, it may not be useful if the locations of targets have some degree of stochastic uncertainties. A statistical approach using the sample statistics (mean and covariance matrix) of given locations of targets can be employed to instantly find an ellipse with a probabilistic guarantee at a central station. Given sample points (targets) or position measurements $p_1, \ldots, p_n \in \mathbb{R}^2$ with an error, the sample mean, $m \in \mathbb{R}^2$ and sample covariance matrix $C \in \mathbb{R}^{2\times 2}$ are respectively calculated as

$$\begin{aligned} m &= \frac{1}{n}\sum_{i=1}^{n} p_i, \\ C &= \frac{1}{n-1}\sum_{i=1}^{n} (p_i - m)(p_i - m)^T, \end{aligned} \tag{4}$$

where C is the covariance. For a positive definite symmetric covariance $C = C^T > 0$, the statistical ellipse can be denoted by $\mathcal{E}(m, C)$:

$$\mathcal{E}(m, C) = \left\{x : (x-m)^T C^{-1}(x-m) \leq 1\right\}. \tag{5}$$

Note that the deterministic approach yields an ellipse with the minimum area but is sensitive to the measurement error and thus cannot guarantee the number of targets inside the ellipse. In contrast, the statistical approach calculates a family of concentric ellipses $\mathcal{E}_\ell(m, C)$ with prescribed probabilities of covering targets [23], [24], [25]:

$$\begin{aligned} \mathcal{E}_\ell(m, C) &= \left\{x : (x-m)^T C^{-1}(x-m) \leq \ell\right\}, \\ P\{\mathbb{X} \in \mathcal{E}_\ell(m, C)\} &= P_\alpha, \end{aligned} \tag{6}$$

where ℓ is the size (i.e., radius) of the ellipse, $\mathbb{X}$ is the random position of the true target, and P_α is the coverage probability that the target lies inside $\mathcal{E}_\ell(m, C)$. Table 1 presents the typical size of a statistical ellipse depending on the prescribed probability. For example, with a coverage probability of $P_\alpha = 0.95$ and $\ell = 5.99 \approx 6$, approximately 95% of true targets are inside the ellipse $\mathcal{E}_6(m, C)$. Other sizes ℓ also have useful interpretations; for example, an ellipse with $\ell = 2.77$ covers 75% of targets. The main advantage of the statistical ellipse over the one obtained by the deterministic approach is that it accounts for the measurement error that inevitably occurs in real-world situations.

Remark 1: If $\mathbb{X} \sim \mathbb{N}(\mathbb{m}, \mathbb{C})$ is a normally distributed random vector with the mean $\mathbb{m} = \mathbb{E}(\mathbb{X})$ and covariance $\mathbb{C} = \mathbb{E}\left[(\mathbb{X} - \mathbb{m})(\mathbb{X} - \mathbb{m})^{\mathrm{T}}\right]$, then the quadratic form $Q(\mathbb{X}) = (\mathbb{X} - \mathbb{m})^{\mathrm{T}}\mathbb{C}^{-1}(\mathbb{X} - \mathbb{m})$ has a chi-squared distribution $\chi^2_2(\alpha)$ with two degrees of freedom [24], [25]:

$$P\left\{Q(\mathbb{X}) \leq \chi^2_2(\alpha)\right\} = 1 - \alpha, \tag{7}$$

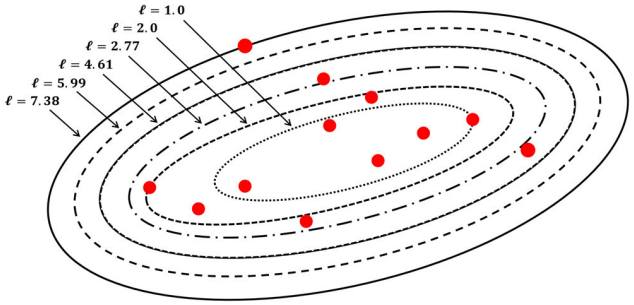

FIGURE 2. Comparison of six concentric statistical ellipses $\mathcal{E}_{7.38}$, $\mathcal{E}_{5.99}$, $\mathcal{E}_{4.61}$, $\mathcal{E}_{2.77}$, $\mathcal{E}_{2.0}$, and $\mathcal{E}_{1.0}$ with different sizes ℓ covering 12, 11, 11, 9, 8, and 5 targets, respectively.

where α is the significance level, $\chi_2^2(\alpha)$ is the upper-tail value of the χ_2^2 distribution, and $1-\alpha$ is the probability that the value of $\mathbb{X}$ lies inside the ellipse determined by $Q(x)$ and $\chi_2^2(\alpha)$. In relation to the present case, (6) and (7) can be compared to see that $P_\alpha = 1-\alpha$ and $\ell = \chi_2^2(\alpha)$ [see Table 1].

Figure 2 shows six statistical ellipses $\mathcal{E}_\ell$ with different coverage probabilities corresponding to sizes $\ell = 1.0$, 2.0, 2.77, 4.61, 5.99 and 7.38 for 12 noisy target position measurements. The largest ellipse $\mathcal{E}_{7.38}$ has a 97.5% probability of covering all true targets.

Remark 2: The above coverage problem also arises in wireless sensor networks. For example, given a set of targets to be covered and a set of mobile sensors, Liang et al. [26] developed a sensor dispatch algorithm maximizing the covered targets under some constraints. Meanwhile, Huang and Savkin [27] deployed drones to offer mobile services with the aim of maximizing the coverage and reducing interference of the cellular network.

C. DISTRIBUTED STATISTICAL APPROACH

Consider a group of N_d drones $D_1, \ldots, D_{N_d}$ that observes a set of L moving targets on the ground with different initial positions and velocities. In general, a number of targets can change over time (i.e., $L = L(t)$). Each drone D_i observes only an individual subset of the targets whose composition and size can change over time within a field of view. Drone i can be assumed to observe L_i moving targets. Then, the measured positions of targets located in the surveillance zone of drone i are given by

$$D_i:\ p_j^{(i)}(t_k) \in \mathbb{R}^2,\ j = 1, \ldots,\ L_i, \tag{8}$$

where $p_j^{(i)} = \left[p_{x,j}^{(i)}, p_{y,j}^{(i)}\right]^T$ is the 2D measured vector with the position components $p_{x,j}^{(i)}$ and $p_{y,j}^{(i)}$ along the x and y axes, respectively and $L_i = L_i(t_k)$ is the number of measurable targets at the time instant t_k. For the sake of simplicity, the time index t_k is omitted. Overlapping between surveillance zones of drones is allowed. In other words, a target can be observed by more than one drone.

Integrating the measurements from all drones obtains

$$\left\{p_j^{(i)}(t_k)\right\}_{j=1}^{L_i},\ i = 1, \ldots, N_d. \tag{9}$$

Thus, the problem becomes finding a common ellipse that covers as many targets as possible. In other words, a distributed algorithm is needed to find the ideal coverage ellipse containing the maximum number of targets. This problem is difficult to solve because of the lack of a central station that can fuse and process all individual measurements in (8). The statistical formulas in Section III-B can be used to calculate the mean and covariance of the measurements taken by each drone $\left\{p_1^{(i)}, p_2^{(i)}, \ldots, p_{L_i}^{(i)}\right\}$ (index i is fixed) separately:

$$\begin{aligned} m^{(i)} &= \frac{1}{L_i}\sum_{j=1}^{L_i} p_j^{(i)}, \\ C^{(i)} &= \frac{1}{L_i - 1}\sum_{j=1}^{L_i}\left(p_j^{(i)} - m^{(i)}\right)\left(p_j^{(i)} - m^{(i)}\right)^T, \\ & \quad i = 1, \ldots, N_d. \end{aligned} \tag{10}$$

In the absence of measurements ($L_i = \emptyset$), $m^{(i)} = C^{(i)} = 0$; in the case of a single measurement ($L_i = 1$), $m^{(i)} = p_1^{(i)}$ and $C^{(i)} = 0$. Thus, a set of individual statistics $\left(m^{(1)}, C^{(1)}\right), \ldots, \left(m^{(N_d)}, C^{(N_d)}\right)$ is obtained for all drones at the time instant t_k.

The following theorem establishes the equivalence of the centralized and distributed statistical approaches to processing the integrated measurements in (9).

Theorem 1: Let N_d *be the number of drones and* $\left\{p_j^{(i)}\right\}_{j=1}^{L_i}$ *be the integrated measurements for* $i = 1, \ldots, N_d$. *The distributed pooled statistics for the mean and covariance can be redefined as*

$$\begin{aligned} m^{dist} &= \frac{1}{L}\sum_{i=1}^{N_d} L_i m^{(i)},\ L = L_1 + \ldots + L_{N_d}, \\ C^{dist} &= \frac{1}{L-1}\sum_{i=1}^{N_d}(L_i - 1)\,C^{(i)} + \frac{1}{L-1}\sum_{i=1}^{N_d} L_i \\ &\quad \times \left(m^{(i)} - m^{dist}\right)\left(m^{(i)} - m^{dist}\right)^T. \end{aligned} \tag{11}$$

Then, m^{dist} *and* C^{dist} *coincide with their centralized versions, respectively*:

$$\begin{aligned} m^{cent} &= \frac{1}{L}\sum_{i=1}^{N_d}\sum_{j=1}^{L_i} p_j^{(i)}, \\ C^{cent} &= \frac{1}{L-1}\sum_{i=1}^{N_d}\sum_{j=1}^{L_i}\left(p_j^{(i)} - m^{cent}\right) \\ &\quad \times \left(p_j^{(i)} - m^{cent}\right)^T. \end{aligned} \tag{12}$$

The proof of Theorem 1 is given in the Appendix. Simple manipulations of (11) then lead to the following corollary.

Corollary 1: The distributed pooled statistics in (11) take the following form for two drones:

$$\begin{aligned} m^{dist} &= \frac{L_1 m^{(1)} + L_2 m^{(2)}}{L_1 + L_2}, \\ C^{dist} &= \frac{(L_1 - 1)\,C^{(1)} + (L_2 - 1)\,C^{(2)}}{L_1 + L_2 - 1} \end{aligned}$$

$$+\frac{L_1L_2}{(L_1+L_2)(L_1+L_2-1)}\times\left(m^{(1)}-m^{(2)}\right)\left(m^{(1)}-m^{(2)}\right)^T. \quad (13)$$

They take the following form for three drones:

$$m^{dist}=\frac{L_1m^{(1)}+L_2m^{(2)}+L_3m^{(3)}}{L},$$
$$C^{dist}=\frac{(L_1-1)C^{(1)}+(L_2-1)C^{(2)}+(L_3-1)C^{(3)}}{L-1}+\frac{L_1\tilde{m}^{(1)}\tilde{m}^{(1)^T}+L_2\tilde{m}^{(2)}\tilde{m}^{(2)^T}+L_3\tilde{m}^{(3)}\tilde{m}^{(3)^T}}{L-1},$$
$$L=L_1+L_2+L_3,$$
$$\tilde{m}^{(i)}=m^{(i)}-m^{dist},\ i=1,2,3. \quad (14)$$

For scalar measurements, (13) coincides with those known in [28]. Thus, the calculated distributed statistics m^{dist} and C^{dist} completely determine the family of coverage ellipses $\{\mathcal{E}_\ell(m^{dist},C^{dist})\}$,

$$\mathcal{E}_\ell=\left\{x:\left(x-m^{dist}\right)^T\left(C^{dist}\right)^{-1}\left(x-m^{dist}\right)\le\ell\right\} \quad (15)$$

with the corresponding coverage probability P_α (see Table 1).

Remark 3: On preprocessing noisy measurements. If a dynamic model of moving targets is known, then linear or nonlinear filtering algorithms such as the Kalman filter can be applied to improve the accuracy of target positions. For example, wind disturbance may cause a drone to deviate from a circular track. Filtering of particularly noisy measurements and their subsequent processing will significantly improve the estimation accuracy of the coverage ellipse.

Remark 4: On network implementation of distributed statistics. After the individual statistics $(m^{(i)},C^{(i)})$ are calculated separately by each onboard computer for $i=1,\ldots,N_d$, the next step involves combining these statistics to calculate a coverage ellipse in fusion center. Fusion center can be achieved using two distinct network configurations. First, referred to as Network with a center at Ground Control Station, where each drone communicates with the station as shown in Figure 3-a. Within this network, each drone transmits its own statistics $(m^{(i)},C^{(i)})$ to the control station. It calculates and transmits the information of coverage ellipse $\mathcal{E}_\ell(m^{dist},C^{dist})$ back to the drones. Second, referred to as Leader-Follower network, where one drone assumes the role of a leader while the others act as followers (see Figure 3-(b)). In this network, each follower drone transmits its own statistics $(m^{(i)},C^{(i)})$ to the leader, which acts as the air fusion center. The leader drone is equipped with sufficient computational resources and power to calculate a common coverage ellipse $\mathcal{E}_\ell=\mathcal{E}_\ell(m^{dist},C^{dist})$ in real-time.

Example of the Leader-Follower network configuration is illustrated in Figure 3-(c). It provides a visual representation of how three drones observe 18 ground targets within their limited viewing angles ($L_1=7$, $L_2=6$ and $L_3=5$) for the following parameters of the individual ellipses:

$$m^{(1)}=[10.8,\ 18.1],\qquad m^{(2)}=[10.7,\ 38,4],$$

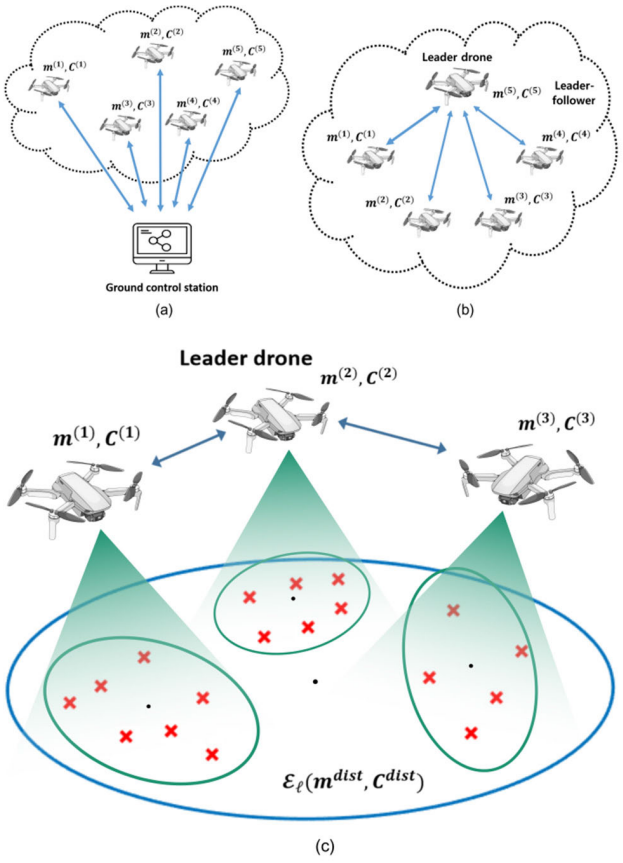

FIGURE 3. Network configurations of drones: (a) Network with a center at Ground Control Station; (b) Leader-follower network; (c) Example scenario of monitoring 12 targets by 3 drones where the second one is leader.

$$C^{(1)}=\begin{bmatrix}0.096&0.040\\0.040&0.057\end{bmatrix},\quad C^{(2)}=\begin{bmatrix}0.062&-0.012\\-0.012&0.122\end{bmatrix}$$
$$m^{(3)}=[30.5,\ 26.5],\qquad C^{(3)}=\begin{bmatrix}0.284&0.026\\0.026&0.059\end{bmatrix},$$
$$m^{(dist)}=[19.8,\ 25.9],\qquad C^{(dist)}=\begin{bmatrix}0.013&-0.005\\-0.005&0.013\end{bmatrix}$$

Within this setup, each drone focuses on its own subset of measurements of moving targets L_i, which may vary in composition and size.

D. GEOMETRY OF THE COVERAGE ELLIPSE

The size ℓ and the axes directions of the family of concentric ellipses $\{\mathcal{E}_\ell\}$ change depending on the selected coverage probability of $P_\alpha=P\{\mathbb{X}\in\mathcal{E}_\ell\}$ and the covariance C^{dist}. C^{dist} and its inverse can be written as

$$C^{dist}=\begin{bmatrix}\sigma_1^2&\sigma_{12}\\\sigma_{12}&\sigma_2^2\end{bmatrix},$$
$$\left(C^{dist}\right)^{-1}=\frac{1}{\sigma_1^2\sigma_2^2\left(1-\rho^2\right)}\begin{bmatrix}\sigma_2^2&-\rho\sigma_1\sigma_2\\-\rho\sigma_1\sigma_2&\sigma_1^2\end{bmatrix}, \quad (16)$$

where $\rho=\sigma_{12}/(\sigma_1\sigma_2)$ is the sample correlation coefficient.

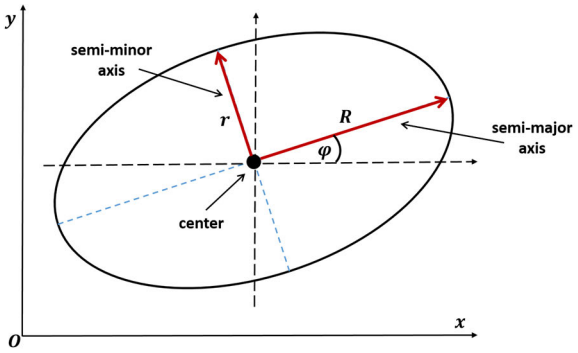

FIGURE 4. Geometry of the ellipse $\mathcal{E}_\ell$.

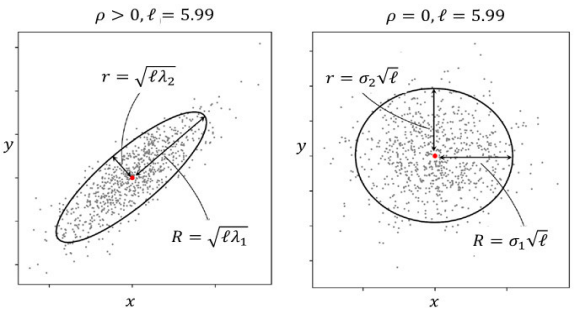

FIGURE 5. Coverage ellipses with $P_\alpha = 0.95$ and their semi-axes when $\rho > 0$ and $\rho = 0$ enclosing randomly generated data points (targets).

The ellipse $\mathcal{E}_\ell$ is centered at $m^{dist} \in \mathbb{R}^2$ and has the following geometric parameters:

$$\tan(2\varphi) = \frac{2\rho\sigma_1\sigma_2}{\sigma_1^2 - \sigma_2^2},\ R = \sqrt{\ell\lambda_1},\ r = \sqrt{\ell\lambda_2},$$
$$\lambda_1 = \frac{1}{2}\left(\sigma_1^2 + \sigma_2^2\right) + \sqrt{\left(\sigma_1^2 - \sigma_2^2\right)^2 + 4\sigma_{12}^2},$$
$$\lambda_2 = \frac{1}{2}\left(\sigma_1^2 + \sigma_2^2\right) - \sqrt{\left(\sigma_1^2 - \sigma_2^2\right)^2 + 4\sigma_{12}^2}, \quad (17)$$

where the angle φ, the length R of semi-major axis, and the length r of semi-minor axis are illustrated in Figure 4. Also, (λ_1, e_1) and (λ_2, e_2) are the eigenvalue-eigenvector pairs of C^{dist}. Note again that the size $\ell = \ell(P_\alpha)$ of the ellipse depends on the coverage probability of P_α according to the chi-square distribution in Table 1.

Figure 5 displays the coverage ellipse $\mathcal{E}_\ell$ with $P_\alpha = 0.95$ and $\ell = 5.99$ (see Table 1), when the target position components along the x and y axes are positively correlated ($\rho > 0$) and uncorrelated $\left(\rho = 0,\ \lambda_1 = \sigma_1^2, \lambda_2 = \sigma_2^2\right)$, respectively. For $\rho > 0$, the semi-major and semi-minor axes of the ellipse are aligned with the rotation axes in the transformed coordinate system. For $\rho = 0$, the axes are parallel to the original coordinate system.

IV. PROPOSED CIRCUMNAVIGATION STRATEGY

The estimated coverage ellipse $\mathcal{E}_\ell\left(m^{dist}, C^{dist}\right)$ can then be used to formulate the proposed circumnavigation strategy. The objective of the strategy is to guide and control a group of drones to monitor all targets within the coverage ellipse. The proposed strategy is an extension of the previousstrategy for using multiple drones to track a single target [12]. Figure 6 presents an overview of the proposed strategy for monitoring multiple targets, which can be divided into four blocks. Block 1 comprises the previously described distributed statistical approach to estimate the coverage ellipse $\mathcal{E}_\ell$. In Block 2, the ellipse is used to calculate a tilted circular orbit $\mathcal{C}$ for monitoring targets. In Block 3, a guidance law is designed based on vector fields. In Block 4, each drone employs integral sliding model control (I-SMC) to track the guidance law in the presence of bounded disturbances.

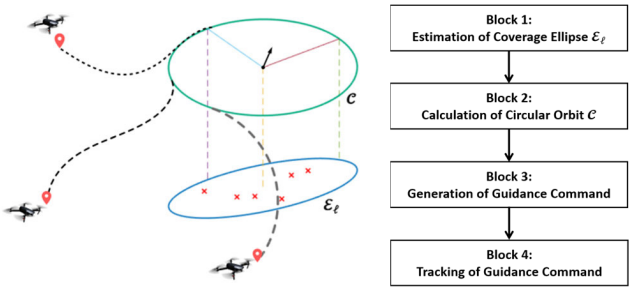

FIGURE 6. Proposed circumnavigation strategy for monitoring multiple targets.

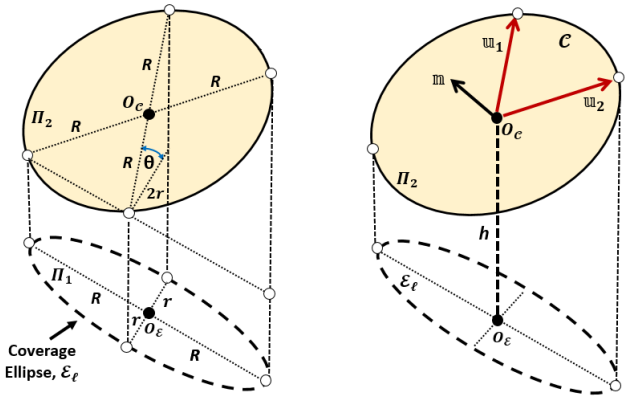

FIGURE 7. Coverage ellipse as an orthogonal projection of a tilted circle.

A. BLOCK 1: COVERAGE ELLIPSE

The common coverage ellipse $\mathcal{E}_\ell\left(m^{dist}, C^{dist}\right)$ and its geometry has been described above in (10), (11) and (15)-(17).

B. BLOCK 2: TILTED CIRCULAR ORBIT

The coverage ellipse $\mathcal{E}_\ell$ represents an orthogonal projection of the tilted circular orbit $\mathcal{C}$ for surveillance as illustrated in Figure 7. Before the proposed strategy can be described, several terms need to be defined:

- Π_1 and Π_2 are the ground and orbit planes, respectively.
- h is the altitude of the center of $\mathcal{C}$.
- $O_\mathcal{E}(x_0, y_0, z_0)$ is the center of the ground coverage ellipse $\mathcal{E}_\ell$, with $z_0 = 0$.

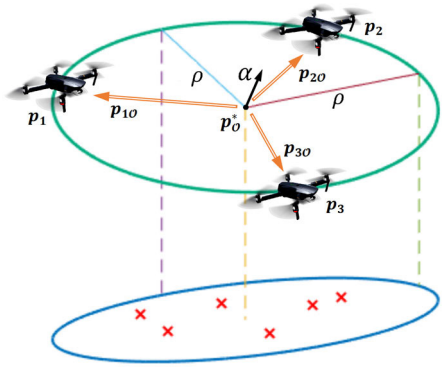

FIGURE 8. Circumnavigation of three drones ($N_d = 3$) for tracking six targets ($L = 6$) on the ground.

- $O_{\mathcal{C}}\,(x_1, y_1, z_1)$ is the center of the circular orbit $\mathcal{C}$, with $x_1 = x_0, y_1 = y_0, z_1 = h$.
- $\mathbb{u}_1$ and $\mathbb{u}_2$ are the orthogonal vectors in the orbit plane Π_2 such that $\mathbb{u}_1 \perp \mathbb{u}_2,\ \|\mathbb{u}_1\| = \|\mathbb{u}_2\| = R$.
- $\mathbb{m}$ is the normal vector to the orbit plane Π_2.
- θ is the tilt angle, implying that $\cos(\theta) = \frac{r}{R}$.

Then, the circular orbit $\mathcal{C}$ is completely determined by the two orthogonal unit vectors $\left(\mathbb{v}_1 = \frac{\mathbb{u}_1}{\|\mathbb{u}_1\|} \text{ and } \mathbb{v}_2 = \frac{\mathbb{u}_2}{\|\mathbb{u}_2\|}\right)$, and the center $O_{\mathcal{C}}\,(x_1, y_1, z_1)$ as follows:

$$\mathcal{C}: \begin{cases} x(\varphi) = x_1 + R\cos(\varphi)\, v_{1x} + R\sin(\varphi)\, v_{2x}, \\ y(\varphi) = y_1 + R\cos(\varphi)\, v_{1y} + R\sin(\varphi)\, v_{2y}, \\ z(\varphi) = z_1 + R\cos(\varphi)\, v_{1z} + R\sin(\varphi)\, v_{2z}, \end{cases}$$
$$\mathbb{v}_1 = \left[v_{1x}, v_{1y}, v_{1z}\right]^T,\ \mathbb{v}_2 = \left[v_{2x}, v_{2y}, v_{2z}\right]^T,$$
$$\varphi \in [0, 2\pi]\,. \tag{18}$$

The unit normal vector of the circular orbit, $\mathbb{m} = \mathbb{m}\left(n_x, n_y, n_z\right)$, can be determined as $\mathbb{m} = \mathbb{v}_1 \mathrm{x}\, \mathbb{v}_2$.

C. BLOCK 3: GENERATION OF GUIDANCE COMMAND

Each drone is modeled as a double-integrator (assuming fast attitude dynamics), commonly used in the literature, such as in [12], [14], [29], and [30]:

$$\ddot{p}_i(t) = u_i(t) + \eta_i(t),$$
$$i \in \mathcal{N} \triangleq \{1,\ 2,\ \ldots,\ N_d\}\,, \tag{19}$$

where $p_i(t),\ u_i(t),\ \eta_i(t) \in \mathbb{R}^3$ represent the position, the control, and the (bounded) disturbance inputs of drone i, respectively.

The centered point of the available tilted circular orbit is denoted by $p^*_{\mathcal{O}}(t) \in \mathbb{R}^3$. The position vector of drone $p_i(t)$ consists of $x,\ y,\ z-$ axis coordinates, and the control input $u_i(t)$ is be designed for the tilted circumnavigation around the center of orbit $p^*_{\mathcal{O}}(t)$ as shown in Figure 8 while satisfying the following three conditions:

1) All drones must reach the tilted circle plane:

$$\lim_{t\to\infty} \alpha(t)^T (p^*_{\mathcal{O}}(t) - p_i(t)) = \lim_{t\to\infty} \alpha^T p_{i\mathcal{O}}(t) = 0,\ \forall i \in \mathcal{N}, \tag{20}$$

where $\alpha(t) \in \mathbb{R}^3$ is the time-varying unit normal vector $\alpha(t) \triangleq \mathbb{m}\,(\mathrm{t})$ of the tilted circle determined in Section IV-B, and $p_{i\mathcal{O}}(t) = p^*_{\mathcal{O}}(t) - p_i(t)$ denotes the relative position between drone i and the center of orbit $p^*_{\mathcal{O}}(t)$;

2) Each drone must turn around the circle's center with the radius of $\rho(t)$ ($= R$ in Section IV-B):

$$\lim_{t\to\infty} |\left(\left\|p^*_{\mathcal{O}}(t) - p_i(t)\right\| - \rho(t)\right)| = 0,\ \forall i \in \mathcal{N} \tag{21}$$

and

3) Drones must avoid collisions at all times:

$$\left\|p_i(t) - p_j(t)\right\| \geq \delta_0,\ \forall i \in \mathcal{N}, j \in \mathcal{N}_i,\ t \geq 0,$$
$$\mathcal{N}_i \triangleq \left\{i_1, i_2, \ldots, i_{L_i}\right\}, \tag{22}$$

where δ_0 is the minimally required inter-drone (Euclidean) distance and $\mathcal{N}_i$ represents the set of drones $D_{i_1},\ldots,D_{i_{L_i}}$, that can communicate with the drone i as its neighbor.

A guidance command based on vector fields is generated for the drones to join the tilted circular orbit and follow it around the targets. The guidance logic was previously proposed in [12], and it is briefly summarized here. To satisfy the three conditions in (20)–(22), the following velocity command $v^r_i(t)$ is generated for each $i \in \mathcal{N}$:

$$v^r_i = v^{(1)}_i + v^{(2)}_i + v^{(3)}_i + v^*_{\mathcal{O}} \tag{23}$$

where

$$v^{(1)}_i = -k_1 \nabla_i V_1, \tag{24}$$
$$v^{(2)}_i = -k_2 \nabla_i V_2 + k_0 \|P_\alpha p_{i\mathcal{O}}\| \left(\alpha \times \varphi^\alpha_i\right), \tag{25}$$
$$v^{(3)}_i = -k_3 \|P_\alpha p_{i\mathcal{O}}\| \nabla_i V_3. \tag{26}$$

The velocity command guidance is calculated by multiplying the gradient of individual potential functions with positive constants or tuning gains (i.e., k_0, k_1, k_2, k_3). The gain k_0 affects the speed at which a drone orbits around the targets. Based on the relative importance of the three conditions, the other gains are calculated. Zhong et al. [31] provides a more in-depth explanation of the tuning gains and the theoretical evidence of convergence for (24)–(26). $v^*_{\mathcal{O}}(t)$ is the velocity of the center of the circular orbit $P_\alpha = I_3 - \alpha\alpha^T$, I_3 is the identity 3×3 matrix, and $\varphi^\alpha_i = \frac{P_\alpha p_{i\mathcal{O}}}{\|P_\alpha p_{i\mathcal{O}}\|}$ is a vector that represents the projection of 3D axis coordinates onto the plane of the tilted circle. $V_1,\ V_2$, and V_3 are the potential functions defined in [12] as follows:

$$V_1 = \frac{1}{2} \sum\nolimits_{i\in\mathcal{N}} (\alpha^T p_{i\mathcal{O}})^2, \tag{27}$$
$$V_2 = \frac{1}{2} \sum_{i\in\mathcal{N}} (\|P_\alpha p_{i\mathcal{O}}\| - \rho)^2, \tag{28}$$
$$V_3 = \frac{1}{2} \sum\nolimits_{i\in\mathcal{N}} \sum\nolimits_{j\in\mathcal{N}_i} a_{ij}\xi(\left\|\varphi^\alpha_i - \varphi^\alpha_j\right\|^2). \tag{29}$$

Here, a_{ij} is an element of the weighted adjacency matrix describing a network topology of drones. $a_{ii} = 0,\ a_{ij} = 1,\ i \neq j,\ j \in \mathcal{N}_i$ and $a_{ij} = 0,\ j \notin \mathcal{N}_i$; $\xi = \xi(x)$ is a scalar function with the argument $x > \delta$, and $\xi(x)$ tends to infinity as x gets close to δ. For instance, $\xi(x) = -\ln\left(x - \delta^2\right)$,

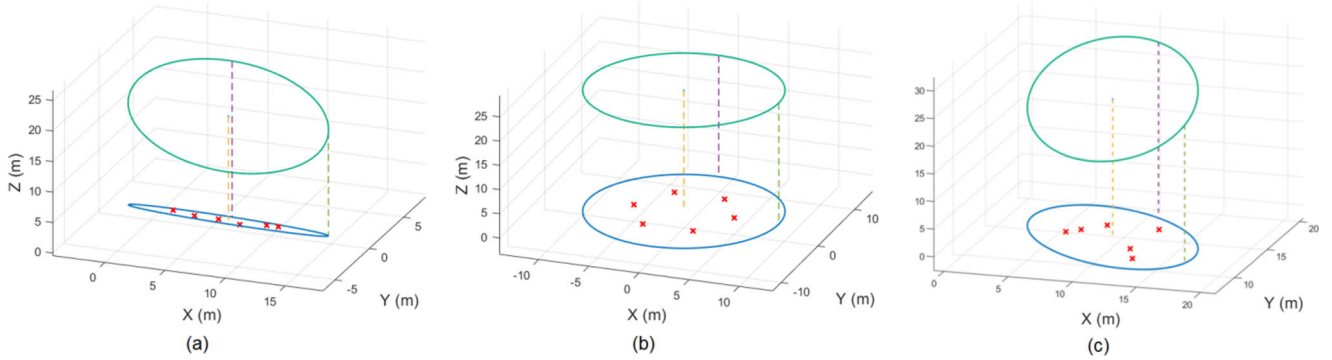

FIGURE 9. Three shapes of coverage ellipses on the ground and the corresponding circular orbits. Scenario I: $R \gg r,\ \theta \approx 90^0$, (b) Scenario II: $R \approx r,\ \theta \approx 0^0$, (c) Scenario III: General case.

where $x = \left\|\varphi_i^\alpha - \varphi_j^\alpha\right\|^2$ can be chosen to satisfy the aforementioned properties. Then, the gradient of each potential function $\nabla_i V_j = \left(\frac{\partial V_j}{\partial p_{i\mathcal{O}}}\right)^{\mathrm{T}}$ is calculated for $j = 1, 2, 3$. Finally, the following position guidance command for each drone can be obtained by integrating the velocity guidance command according to (23) over time:

$$p_i^r(t) = \int_0^t v_i^r(s)ds. \tag{30}$$

D. BLOCK 4: TRACKING GUIDANCE COMMAND

The position guidance command is tracked by I-SMC as in the previous design [12]. Each drone is equipped with an I-SMC law, which enables finite-time convergence to a predetermined sliding surface even in the presence of bounded disturbances. The positional error and related sliding variable for drone i can be defined as follows [12]:

$$e_i = p_i^r - p_i, \tag{31}$$
$$\sigma_i = \dot{e}_i - ce_i, \tag{32}$$

where $c > 0$ is a positive constant that controls the speed of the convergence to $e_i = 0$.

Then, the I-SMC control input is designed as follows:

$$u_i = u_i^{(1)} + u_i^{(2)}, \tag{33}$$
$$u_i^{(1)} = \tau \mathrm{sign}(s_i), \tag{34}$$
$$u_i^{(2)} = c\dot{e}_i + k\sigma_i, \tag{35}$$

where

$$s_i = \sigma_i + \int_0^t k\sigma_i dt, \tag{36}$$

$$\mathrm{sign}(x) = \begin{cases} -1, & \text{if } x < 0; \\ 1, & \text{if } x > 0. \end{cases} \tag{37}$$

The tuning parameters in the I-SMC law are represented by τ and k, where τ is determined by the size of the uncertain signal as demonstrated by the proof for Theorem 1 in [12] and k controls the convergence speed to $\sigma_i = 0$. The purpose of $u_i^{(1)}$ is to initiate the sliding phase immediately without a reaching phase, and $u_i^{(2)}$ ensures that s_i converges to 0 in finite time. This in turn results in the asymptotic convergence of σ_i and e_i to zero [32].

Remark 5: On the convergence of the control logic. The convergence behavior of the proposed control logic is formally proven in [12] for when the circle's radius and unit normal vector remain constant. This implies that the convergence result is applicable for cases where the circle's radius and unit normal vector vary slowly over time. Computer simulations were performed to verify this implication.

V. SIMULATION STUDY

A. SIMULATION SCENARIOS

Numerical simulations were performed to demonstrate the Effectiveness of the proposed strategy for three drones ($N_d = 3$) to circumnavigate six moving targets ($L = 6$) within a time-varying coverage ellipse ($\mathcal{E}_\ell(t)$) on the ground by following a tilted circular orbit ($\mathcal{C}(t)$) . Three different scenarios were considered to yield coverage ellipses with different shapes.

In Scenario I, the major axis of the coverage ellipse was significantly larger than the minor axis ($R \gg r$), which resulted in a tilt angle θ for the circular orbit of around 90°, as shown in Figure 9-(a). In Scenario II, the major and minor axes of the coverage ellipse had similar lengths ($R \approx r$), which resulted in the ellipse and corresponding circular orbit being nearly parallel to the xy plane owing to a tilt angle $\theta \approx 0$ as illustrated in Figure 9-b. Scenario III represented a typical case where the tilt angle is somewhere between the two extremes of the previous scenarios, as shown in Figure 9-(c). The simulations were performed to confirm that the proposed strategy meets the conditions in (20)–(22) as in [12]. The required control inputs were also checked to confirm that the proposed strategy does not need excessive inputs to track multiple targets. For example, using an elliptic orbit would obviously require excessive control inputs at the corners associated with the major axis in Scenario I.

TABLE 2. Initial positions of drones and targets.

№		Drone position	Target position	
Scenario I	$p_{1,0} = [-5, -5, 0]^T$	$\tilde{p}_{1,0} = [1, 1.4, 0]^T$	$\tilde{p}_{4,0} = [7, 0.6, 0]^T$
	$p_{2,0} = [-10, 5, 0]^T$	$\tilde{p}_{2,0} = [3, 1, 0]^T$	$\tilde{p}_{5,0} = [9, 1, 0]^T$
	$p_{3,0} = [10, -5, 0]^T$	$\tilde{p}_{3,0} = [5, 1, 0]^T$	$\tilde{p}_{6,0} = [10, 1, 0]^T$
Scenario II	$p_{1,0} = [-15, -10, 0]^T$	$\tilde{p}_{1,0} = [5, 0, 0]^T$	$\tilde{p}_{4,0} = [-5, 0, 0]^T$
	$p_{2,0} = [-15, 0, 0]^T$	$\tilde{p}_{2,0} = [2.5, 4.33, 0]^T$	$\tilde{p}_{5,0} = [-2.5, -4.33, 0]^T$
	$p_{3,0} = [10, -5, 0]^T$	$\tilde{p}_{3,0} = [-2.5, 4.33, 0]^T$	$\tilde{p}_{6,0} = [2.5, -4.33, 0]^T$
Scenario III	$p_{1,0} = [-15, 20, 45]^T$	$\tilde{p}_{1,0} = [-1, 5.5, 0]^T$	$\tilde{p}_{4,0} = [-4.5, 10, 0]^T$
	$p_{2,0} = [5, 30, 55]^T$	$\tilde{p}_{2,0} = [-8, 10, 0]^T$	$\tilde{p}_{5,0} = [5.5, 5, 0]^T$
	$p_{3,0} = [-10, -10, 60]^T$	$\tilde{p}_{3,0} = [-6.5, -1.5, 0]^T$	$\tilde{p}_{6,0} = [8, 10, 0]^T$

B. TARGET MODELS

The six ground targets were each modeled by the following discrete-time (i.e., nearly constant velocity) equation:

$$\begin{aligned} X_j(t_{k+1}) &= FX_j(t_k) + G\zeta_j(t_k), \\ t_k &= k\Delta t,\ k = 0, 1, \ldots, k_T, \\ F &= \begin{bmatrix} 1 & 0 & \Delta t & 0 \\ 0 & 1 & 0 & \Delta t \\ 0 & 0 & 1 & 0 \\ 0 & 0 & 0 & 1 \end{bmatrix},\ G = \begin{bmatrix} 0 & 0 \\ 0 & 0 \\ 1 & 0 \\ 0 & 1 \end{bmatrix}, \\ \zeta_j(t_k) &\sim N\left(0, Q_j\right),\ j = 1, \ldots, L\ (L = 6) \end{aligned} \quad (38)$$

where Δt is the sampling interval and k_T is the terminal time index. $X_j(t_k)$ is the state of target j defined by $X_j(t_k) = \left[\tilde{p}_j(t_k)^T, \tilde{v}_j(t_k)^T\right]^T$, where $\tilde{p}_j(t_k) = \left[p_{x,j}^{\sim}(t_k), p_{y,j}^{\sim}(t_k)\right]^T$ and $\tilde{v}_j(t_k) = \left[v_{x,j}^{\sim}(t_k), v_{y,j}^{\sim}(t_k)\right]^T$ denote the position and corresponding velocity on the horizontal plane, respectively, of target j. $\zeta_j(t_k) = \left[\zeta_{x,j}(t_k), \zeta_{y,j}(t_k)\right]^T$ is a vector of Gaussian process noise with the covariance $Q_j = q_j I_2$. The initial conditions are set as $X_j(t_0) = \overline{X_j}$ for $j = 1, \ldots, L$.

Each drone D_i $(i = 1, 2, 3)$ was assumed equipped with devices to receive all targets' state information continuously. Then, the noisy vector measurement $Z^{(i)}(t_k) \in \mathbb{R}^{12}$ can be described as

$$Z^{(i)}(t_k) = \begin{bmatrix} z_1^{(i)}(t_k) \\ \vdots \\ z_6^{(i)}(t_k) \end{bmatrix} = \begin{bmatrix} \tilde{p_1}(t_k) + \vartheta_1^{(i)}(t_k) \\ \vdots \\ \tilde{p_6}(t_k) + \vartheta_6^{(i)}(t_k) \end{bmatrix}, \quad (39)$$

where $z_j^{(i)}(t_k) \in \mathbb{R}^2$ is the position measurement of target j received by drone i and $\vartheta_j^{(i)}(t_k) \in \mathbb{R}^2$ is the zero-mean Gaussian measurement noise with the covariance $R_j^{(i)} = d_{i,j} I_2$, $i = 1, 2, 3$; $j = 1, \ldots, 6$. Based on the distributed pooled statistics in (14), for the three drones over the leader-follower network configuration (see Figure 3-(c)) and the simulated measurements $Z^{(i)}(t_k)$, $i = 1, 2, 3$, the distributed ellipse $\mathcal{E}_\ell(t_k)$ with the size $\ell = 7.38$ covers all the targets. This yields the corresponding tilted circular orbit $\mathcal{C}(t_k)$ with the center $p_O^*(t_k)$, $k = 1, 2, \ldots, k_T$.

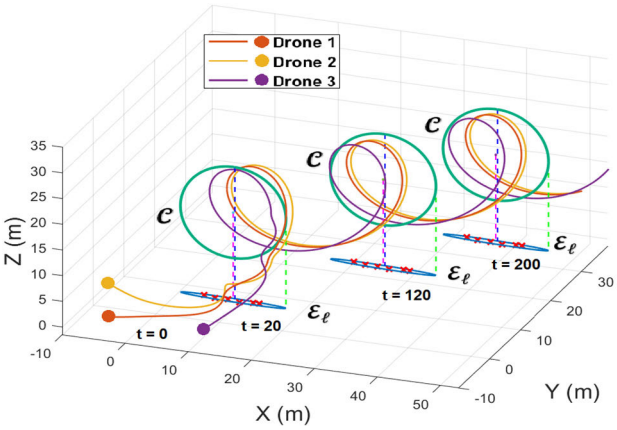

FIGURE 10. 3D trajectories of drones in Scenario I at time instants 0, 20, 120, and 200 s and tuning parameters k_0=k_1= 0.1, k_2= 0.1, and k_3= 0.05.

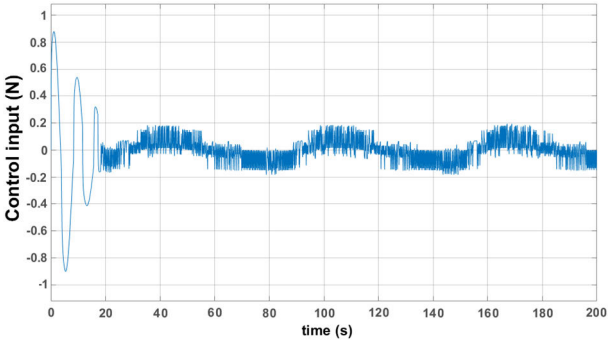

FIGURE 11. Control inputs for the third drone in Scenario I.

C. SIMULATION PARAMETERS

In Scenarios I-III the initial positions of drones $p_i(t_0) \triangleq p_{i,0}$, $i = 1, 2, 3$ and targets $\tilde{p_j}(t_0) \triangleq \tilde{p_{j,0}}, j = 1, \ldots, 6$ are selected as in Table 2.

The following simulation parameters are common for all three scenarios:

- The initial target velocities are set to $\tilde{v_j}(t_0) = [0.5,\ 0.5]^T$ for $j = 1, \ldots, 6$.
- The minimal distance required between drones was set to δ_0= 0.5 m.
- The process noise $\left(Q_j\right)$ and measurement noise $\left(R_j^{(i)}\right)$ covariances are modeled with equal variances $q_j = 4.47 \cdot 10^{-4}$ and $d_{i,j} = 4.47 \cdot 10^{-3}$, respectively.
- The weighted adjacency matrix element set to $a_{ij} = 1$.
- The bounded disturbance input of drones is assumed to be constant with a strength of $\eta_i = 0.1$.
- The tuning parameters for I-SMC are set to $c = 0.2$, $k = 0.3$, and $\tau = 0.1$.

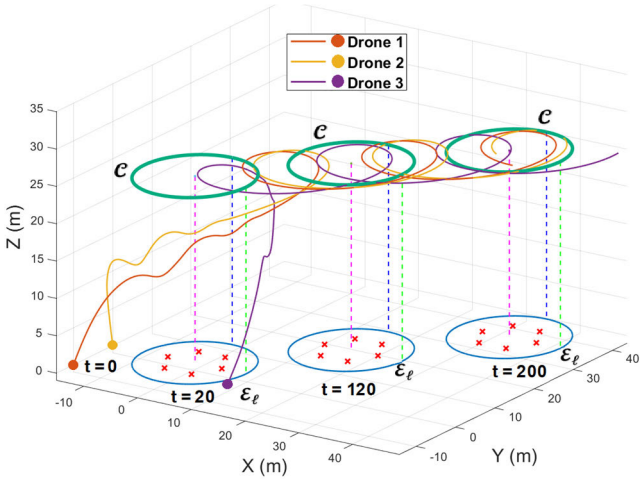

FIGURE 12. 3D trajectories of drones in Scenario II at time instants 0, 20, 120, and 200 s and tuning parameters $k_0{=}k_1{=}0.1$, $k_2{=}0.1$, and $k_3{=}0.05$.

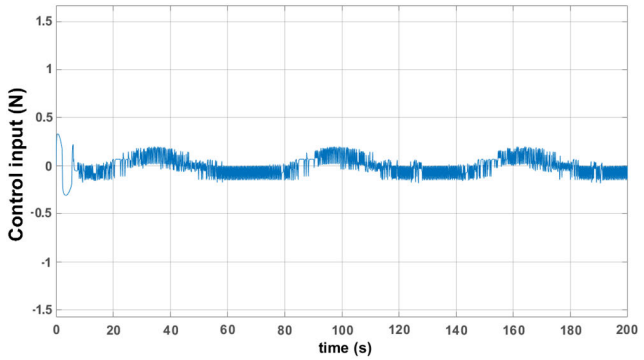

FIGURE 13. Control inputs for the third drone in Scenario II (similar for other drones).

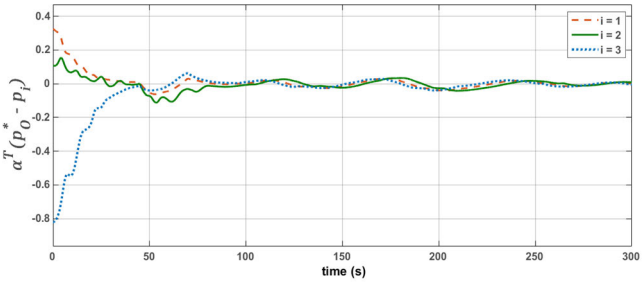

FIGURE 14. Alignment of drones $i = 1, 2, 3$ with the circular orbit in Scenario III as given by $\alpha(t)^T(p_O^*(t){-}p_i(t))$.

- The tuning parameters for the velocity-field guidance command generation are set to $k_0 = k_1 = 0.1$, $k_2 = 0.5$ and $k_3 = 0.05$.

D. SIMULATION RESULTS

1) SCENARIO I

Scenario I (Figure 9-(a)) is representative of a convoy-like configuration in which the targets move in a line. This scenario corresponds to $R \gg r$, so the tilt angle θ of the circular orbit approaches 90°, and the drones may need to change

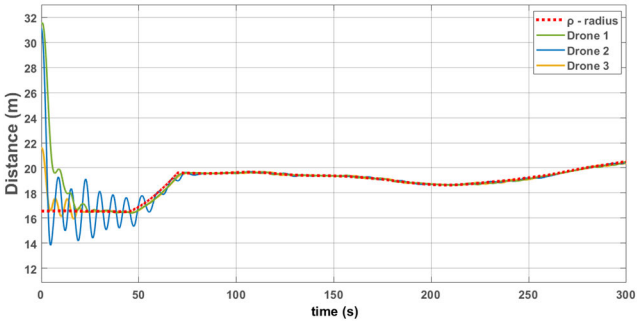

FIGURE 15. Distance $\rho_i(t)$ between the center of the circular orbit and drones $i = 1, 2, 3$ in Scenario III.

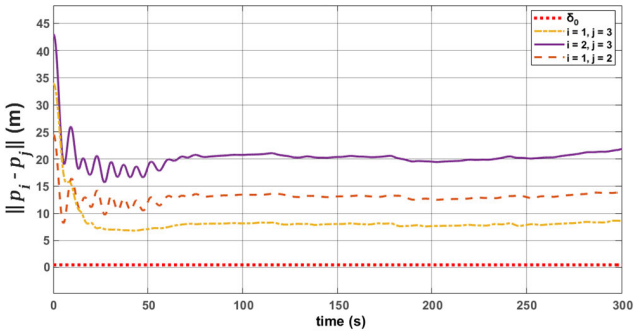

FIGURE 16. Inter-drone distances $\|p_i(t){-}p_j(t)\|$, $i, j = 1, 2, 3; i{\neq}j$ in Scenario III.

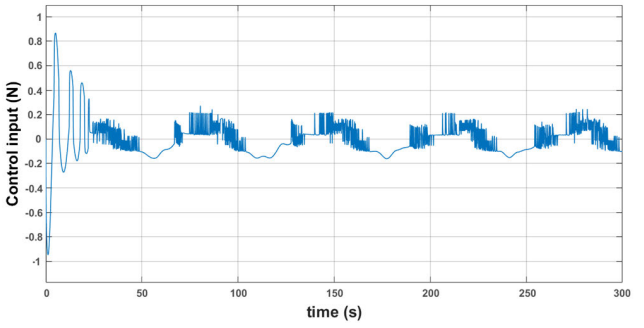

FIGURE 17. Control input of third drone in Scenario III.

altitude to circumnavigate the circular orbit. Note that following the coverage ellipse up to a certain altitude would result in excessive or infeasible control inputs around the corners associated with the major axis. Figures 10 and 11 show the simulation results for Scenario I. Figure 10 illustrates the convoy-like configuration of moving targets and the coverage ellipse with its major axis $R = 8.54$ m and minor axis $r = 0.64$ m at the time instant of 20 s. The corresponding tilt angle of the circular orbit is $\theta = 85.65^{\circ}$. The three drones followed smooth trajectories as they followed the circular orbit. All three drones satisfied the conditions in (20)–(22).

Figure 11 shows the control inputs for the third drone, which were similar for the other drones. Moderate control inputs were sufficient for the three drones to circumnavigate around the six moving targets while maintaining smooth and

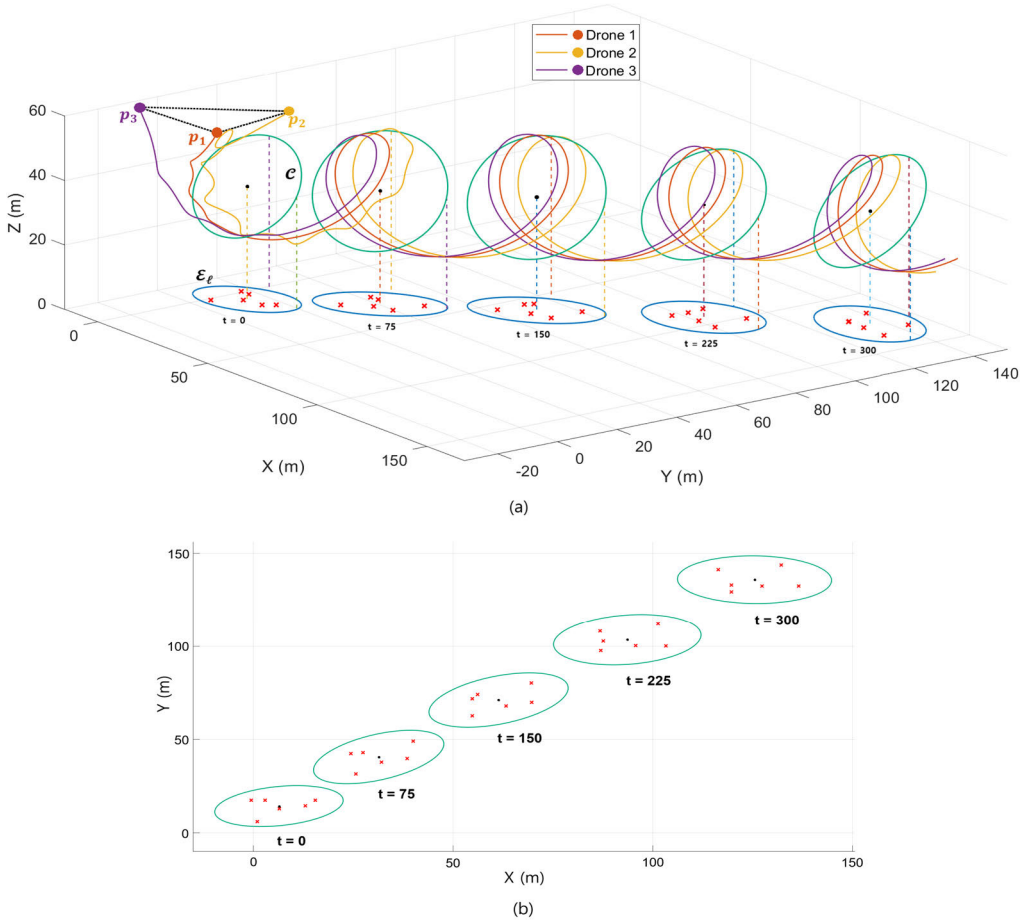

FIGURE 18. (a) 3D trajectories of drones in Scenario III at five different time instants (0, 75, 150, 225, and 300 s). The vertices of the dashed triangles $\Delta p_1 p_2 p_3$ represent the initial positions of drones and (b) 2D visualization of coverage ellipse change for case (a).

TABLE 3. Comparison with prior works in the literature.

Refs.	Multiple drones	Multiple targets	Circumnavigation: circular orbit	Time-varying circular orbit	Collision avoidance	Robustness
[12]	O	X	O	X	O	O
[14]	O	O	O	X	X	V
[29]	X	X	X	X	X	X
[30]	O	X	X	X	X	O
Present work	O	O	O	O	O	O

O - considered, X - not considered, V - not proven

accurate trajectories at a reduced energy consumption. Thus, the drones smoothly circumnavigated a highly inclined orbit plane while monitoring the moving targets

2) SCENARIO II

In Scenario II, the coverage ellipse is close to a circle in shape, and the tilt angle θ approaches 0^o, which means that the orbit plane is not inclined. As shown in Figure 12, the major and minor radii of the coverage ellipse at $t_k = 20$s ($R = 9.479$ m and $r = 9.478$ m) are similar, and the corresponding tilt angle is $\theta = 0.2^o$. The three drones smoothly navigated around the circular orbit while maintaining a suitable distance from the center. The drones smoothly reached the orbit plane and executed turns while maintaining their desired positions, which confirmed the effectiveness of the proposed strategy in Scenario II.

Figure 13 shows that moderate control inputs were sufficient for the drones to follow the circular orbit with $\theta \approx 0^o$. A comparison between Scenarios I and II (i.e., Figures 11 and 13) shows that the required control inputs to

achieve orbit decreased with a decreasing tilt angle. In addition, the control inputs along the orbit were relatively similar for Scenarios I and II. These results confirm that the proposed strategy is effective for any tilt angle of the orbit plane.

3) SCENARIO III

To further demonstrate the successful implementation of the desired circumnavigation and validate the effectiveness of the proposed approach, additional figures are presented, along with simulations confirming that the conditions in (20)-(22) were satisfied.

Figure 14 shows the attempt of each drone to reach the orbit plane of the tilted circle $\mathcal{C}$. As each drone approached the orbit plane, $\alpha(t)^T(p_O^*(t) - p_i(t))$ tended to zero. This demonstrates that the drones successfully aligned with the desired orbit. Figure 15 shows the drones following the tilted circular orbit while maintaining a distance $\rho(t)$ from the center, where $\rho(t)$ represents the radius of the circular orbit.

Figure 16 shows that no collisions occurred between the drones throughout the circumnavigation process. The inter-drone distances were consistently maintained above the minimum value of $\delta_0 = 0.5\text{m}, (\text{i.e.} \left\| p_i(t) - p_j(t) \right\| > \delta_0,\ i \neq j)$. This confirms that the proposed approach ensures safe circumnavigation. Figure 17 shows the control inputs of the third drone. Note that the oscillatory behavior is due to the inherent characteristics (high-speed switching between positive and negative maximum control inputs) of I-SMC technique. Moderate control inputs were sufficient to achieve successful circumnavigation. Figure 18 presents the 3D trajectories of all three drones during the circumnavigation. The proposed strategy effectively guided the drones to follow a tilted circular orbit while maintaining the prescribed inter-drone distance and avoiding collisions even with disturbances.

These findings provide strong evidence of the robustness of the proposed strategy in practical applications. The simulation results confirm that the drones achieved successful tilted circumnavigation while avoiding collisions in all scenarios.

Before closing this section, we have conducted a comparative analysis between the proposed approach and existing works in the literature where drones are modeled as double-integrator (see (19)). The proposed approach is specifically designed to address the complex challenges associated with the application of multiple drones in circumnavigating a time-varying circular orbit while avoiding collisions and maintaining robustness against disturbances, all essential for completing the titled circumnavigation around multiple targets. Table 3 highlights the distinct advantages of the proposed approach over the existing works by addressing these complex challenges.

VI. CONCLUSION

This paper presents a novel strategy for multiple drones to circumnavigate multiple moving targets while avoiding collision. Instead of orbiting a coverage ellipse defined on the ground that encloses the given targets, the proposed strategy is to orbit a tilted circle defined in the air whose projection is identical to the shape of the coverage ellipse. This allows the drones to track the tilted circle at an almost constant velocity while changing altitude slightly. The tilted circular orbit is estimated by a distributed probabilistic approach that is robust against measurement noise. Then, a vector field-based guidance law is coupled with I-SMC to allow the drones to track the tilted circular orbit. Simulations were performed to show that the proposed strategy satisfied the three necessary conditions (20)–(22) for successful tilted circumnavigation in different scenarios.

Future work shall involve improving the control strategy to accommodate communication delays between drones and the situation where targets quickly change the shape of their formation, and to introduce Kalman filter to improve the estimation accuracy of the coverage ellipse. Also, actual drones shall be used to perform practical evaluation of the proposed control strategy. More sophisticated drone and environmental models shall be introduced to improve the practicality of the proposed approach.

APPENDIX

Proof of Theorem 1 Derivation of (11) and establishing its equivalence with (12). Manipulating the centralized mean yields

$$\begin{aligned} m^{cent} &= \frac{1}{L}\sum_{i=1}^{N_d}\sum_{j=1}^{L_i} p_j^{(i)} \\ &= \frac{1}{L}\sum_{i=1}^{N_d} L_i \left(\frac{1}{L_i}\sum_{j=1}^{L_i} p_j^{(i)}\right) \\ &= \frac{1}{L}\sum_{i=1}^{N_d} L_i m^{(i)}. \end{aligned} \tag{A.1}$$

This completes the proof of the equivalence between (11) and (12) in terms of the mean. Then, manipulating the centralized covariance yields

$$\begin{aligned} &C^{cent} \\ &= \frac{1}{L-1}\sum_{i=1}^{N_d}\sum_{j=1}^{L_i}\left(p_j^{(i)} - m^{cent}\right)\left(p_j^{(i)} - m^{cent}\right)^T \\ &= \frac{1}{L-1}\sum_{i=1}^{N_d}\sum_{j=1}^{L_i}\left[\left(p_j^{(i)} - m^{(i)}\right) + \left(m^{(i)} - m^{cent}\right)\right] \\ &\quad \times \left[\left(p_j^{(i)} - m^{(i)}\right) + \left(m^{(i)} - m^{cent}\right)\right]^T \\ &= \frac{1}{L-1}\sum_{i=1}^{N_d}\left\{\sum_{j=1}^{L_i}\left[\left(p_j^{(i)} - m^{(i)}\right)\left(p_j^{(i)} - m^{(i)}\right)^T\right]\right. \\ &\quad + \sum_{j=1}^{L_i}\left[\left(m^{(i)} - m^{cent}\right)\left(p_j^{(i)} - m^{(i)}\right)^T\right] \\ &\quad + \sum_{j=1}^{L_i}\left[\left(p_j^{(i)} - m^{(i)}\right)\left(m^{(i)} - m^{cent}\right)^T\right] \\ &\quad \left. + \sum_{j=1}^{L_i}\left[\left(m^{(i)} - m^{cent}\right)\left(m^{(i)} - m^{cent}\right)^T\right]\right\} \\ &= \frac{1}{L-1}\sum_{i=1}^{N_d}\left(S_1^{L_i} + S_2^{L_i} + S_3^{L_i} + S_4^{L_i}\right), \end{aligned} \tag{A.2}$$

where

$$\begin{aligned} S_1^{L_i} &= \sum_{j=1}^{L_i} \left[\left(p_j^{(i)} - m^{(i)} \right) \left(p_j^{(i)} - m^{(i)} \right)^T \right] \\ &= \frac{L_i - 1}{L_i - 1} \sum_{j=1}^{L_i} \left[\left(p_j^{(i)} - m^{(i)} \right) \left(p_j^{(i)} - m^{(i)} \right)^T \right] \\ &= (L_i - 1)\, C_i \end{aligned} \tag{A.3}$$

$$\begin{aligned} S_2^{L_i} &= \sum_{j=1}^{L_i} \left[\left(m^{(i)} - m^{cent} \right) \left(p_j^{(i)} - m^{(i)} \right)^T \right] \\ &= \sum_{j=1}^{L_i} \left(m^{(i)} p_j^{(i)^T} - m^{cent} p_j^{(i)^T} \right. \\ &\quad \left. - m^{(i)} m^{(i)^T} + m^{cent} m^{(i)^T} \right) \\ &= L_i m^{(i)} m^{(i)^T} - L_i m^{cent} m^{(i)^T} \\ &\quad - L_i m^{(i)} m^{(i)^T} + L_i m^{cent} m^{(i)^T} = 0. \end{aligned} \tag{A.4}$$

Similarly, it can be shown that $S_3^{L_i} = 0$. Next,

$$\begin{aligned} S_4^{L_i} &= \sum_{j=1}^{L_i} \left[\left(m^{(i)} - m^{cent} \right) \left(m^{(i)} - m^{cent} \right)^T \right] \\ &= L_i \left(m^{(i)} - m^{cent} \right) \left(m^{(i)} - m^{cent} \right)^T. \end{aligned} \tag{A.5}$$

Based on (A.3)-(A.5), the centralized covariance in (A.2) is given by

$$\begin{aligned} C^{cent} &= \frac{1}{L-1} \sum_{i=1}^{N_d} (L_i - 1)\, C^{(i)} \\ &\quad + \frac{1}{L-1} \sum_{i=1}^{N_d} L_i \left(m^{(i)} - m^{cent} \right) \left(m^{(i)} - m^{cent} \right)^T \end{aligned} \tag{A.6}$$

Considering the equality from (A.1) of $m^{cent} = m^{dist}$, (A.6) indicates that $C^{cent} = C^{dist}$. This completes the proof of the equivalence between (11) and (12) in terms of the covariance.

ACKNOWLEDGMENT

This work was based on the Mirzobek Malikov's thesis for the master's degree with Gyeongsang National University. An earlier version of this paper was presented in part at the 23rd International Conference on Control, Automation and Systems, Yeosu, Republic of Korea.

REFERENCES

[1] B. Alzahrani, O. S. Oubbati, A. Barnawi, M. Atiquzzaman, and D. Alghazzawi, "UAV assistance paradigm: State-of-the-art in applications and challenges," *J. Netw. Comput. Appl.*, vol. 166, Sep. 2020, Art. no. 102706, doi: 10.1016/j.jnca.2020.102706.

[2] S. Yeom and D.-H. Nam, "Moving vehicle tracking with a moving drone based on track association," *Appl. Sci.*, vol. 11, no. 9, p. 4046, Apr. 2021, doi: 10.3390/app11094046.

[3] J. Hu, H. Niu, J. Carrasco, B. Lennox, and F. Arvin, "Fault-tolerant cooperative navigation of networked UAV swarms for forest fire monitoring," *Aerosp. Sci. Technol.*, vol. 123, Apr. 2022, Art. no. 107494, doi: 10.1016/j.ast.2022.107494.

[4] M. Zhang, H. Wang, and J. Wu, "On UAV source seeking with complex dynamic characteristics and multiple constraints: A cooperative standoff monitoring mode," *Aerosp. Sci. Technol.*, vol. 121, Feb. 2022, Art. no. 107315, doi: 10.1016/j.ast.2021.107315.

[5] P. Chen, Y. Dang, R. Liang, W. Zhu, and X. He, "Real-time object tracking on a drone with multi-inertial sensing data," *IEEE Trans. Intell. Transp. Syst.*, vol. 19, no. 1, pp. 131–139, Jan. 2018.

[6] Y. Wang, H. Wang, J. Wu, Y. Liu, and Y. Lun, "UAV standoff tracking for narrow-area target in complex environment," *IEEE Syst. J.*, vol. 16, no. 3, pp. 4583–4594, Sep. 2022.

[7] Y. Gao, C. Bai, L. Zhang, and Q. Quan, "Multi-UAV cooperative target encirclement within an annular virtual tube," *Aerosp. Sci. Technol.*, vol. 128, Sep. 2022, Art. no. 107800, doi: 10.1016/j.ast.2022.107800.

[8] M. Zhang, J. Jia, and J. Mei, "A composite system theory-based guidance law for cooperative target circumnavigation of UAVs," *Aerosp. Sci. Technol.*, vol. 118, Nov. 2021, Art. no. 107034, doi: 10.1016/j.ast.2021.107034.

[9] E. W. Frew, "Sensitivity of cooperative target geolocalization to orbit coordination," *J. Guid., Control, Dyn.*, vol. 31, no. 4, pp. 1028–1040, Jul. 2008.

[10] S. Huang, Y. Lyu, J. Shi, C. Lin, and Q. Zhu, "Standoff tracking of an unknown object with only distance measurements," *Aerosp. Sci. Technol.*, vol. 132, Jan. 2023, Art. no. 108066, doi: 10.1016/j.ast.2022.108066.

[11] Y. Liu, A. Saeed, M. Z. Shah, L. Wang, and Q.-G. Wang, "Sliding mode lateral stand-off tracking control of finless airship," *Aerosp. Sci. Technol.*, vol. 119, Dec. 2021, Art. no. 107164, doi: 10.1016/j.ast.2021.107164.

[12] Y. Park and Y. Kim, "Circumnavigation of multiple drones under intermittent observation: An integration of guidance, control, and estimation," *Int. J. Aeronaut. Space Sci.*, vol. 23, no. 2, pp. 423–433, Mar. 2022.

[13] K. Chen, G. Qi, Y. Li, and A. Sheng, "Cooperative localization and circumnavigation of multiple targets with bearing-only measurements," *J. Franklin Inst.*, vol. 360, no. 12, pp. 9159–9179, Aug. 2023, doi: 10.1016/j.jfranklin.2022.09.039.

[14] D. Lawrence, E. Frew, and W. Pisano, "Lyapunov vector fields for autonomous UAV flight control," *J. Guid. Control Dyn.*, vol. 31, no. 5, pp. 1220–1229, 2008.

[15] E. W. Frew, D. A. Lawrence, and S. Morris, "Coordinated standoff tracking of moving targets using Lyapunov guidance vector fields," *J. Guid., Control, Dyn.*, vol. 31, no. 2, pp. 290–306, Mar. 2008.

[16] T. Z. Muslimov and R. A. Munasypov, "Coordinated UAV standoff tracking of moving target based on Lyapunov vector fields," in *Proc. Int. Conf. Nonlinearity, Inf. Robot. (NIR)*, Dec. 2020, pp. 1–5, doi: 10.1109/NIR50484.2020.9290189.

[17] D. Li, K. Cao, L. Kong, and H. Yu, "Fully distributed cooperative circumnavigation of networked unmanned aerial vehicles," *IEEE/ASME Trans. Mechatronics*, vol. 26, no. 2, pp. 709–718, Apr. 2021.

[18] D. Li, G. Ma, W. He, S. S. Ge, and T. H. Lee, "Cooperative circumnavigation control of networked microsatellites," *IEEE Trans. Cybern.*, vol. 50, no. 10, pp. 4550–4555, Oct. 2020.

[19] S. Sun, Y. Liu, S. Guo, G. Li, and X. Yuan, "Observation-driven multiple UAV coordinated standoff target tracking based on model predictive control," *Tsinghua Sci. Technol.*, vol. 27, no. 6, pp. 948–963, Dec. 2022.

[20] S. Boyd and L. Vandenberghe, *Convex Optimization*. Cambridge, U.K.: Cambridge Univ. Press, 2004.

[21] M. Todd, *Minimum-Volume Ellipsoids: Theory and Algorithms*. Philadelphia, PA, USA: SIAM, 2016.

[22] P. Kumar and E. A. Yildirim, "Minimum-volume enclosing ellipsoids and core sets," *J. Optim. Theory Appl.*, vol. 126, no. 1, pp. 1–21, Jul. 2005.

[23] L. R. Paradowski, "Uncertainty ellipses and their application to interval estimation of emitter position," *IEEE Trans. Aerosp. Electron. Syst.*, vol. 33, no. 1, pp. 126–133, Jan. 1997.

[24] D. Saville and G. Wood, *Statistical Methods: The Geometric Approach* (Springer Texts in Statistics). New York, NY, USA: Springer, 1991.

[25] T. Wickens, *The Geometry of Multivariate Statistics*. Hillsdale, NJ, USA: Lawrence Erlbaum Associates, 1995.

[26] D. Liang, H. Shen, and L. Chen, "Maximum target coverage problem in mobile wireless sensor networks," *Sensors*, vol. 21, no. 1, p. 184, Dec. 2020, doi: 10.3390/s21010184.

[27] H. Huang and A. V. Savkin, "A method for optimized deployment of unmanned aerial vehicles for maximum coverage and minimum interference in cellular networks," *IEEE Trans. Ind. Informat.*, vol. 15, no. 5, pp. 2638–2647, May 2019.

[28] R. W. R. Baker and J. A. Nissim, "Expressions for combining standard errors of two groups and for sequential standard error," *Nature*, vol. 198, no. 4884, p. 1020, Jun. 1963.

[29] R. Beard, "Quadrotor dynamics and control," *Bringham Young Univ.*, vol. 19, no. 3, pp. 46–56, Feb. 2008.

[30] R. T. Y. Thien and Y. Kim, "Decentralized formation flight via PID and integral sliding mode control," *IFAC-PapersOnLine*, vol. 51, no. 23, pp. 13–15, 2018.

[31] H. Zhong, Y. Wang, Z. Miao, J. Tan, L. Li, H. Zhang, and R. Fierro, "Circumnavigation of a moving target in 3D by multi-agent systems with collision avoidance: An orthogonal vector fields-based approach," *Int. J. Control, Autom. Syst.*, vol. 17, no. 1, pp. 212–224, Jan. 2019.
[32] Y. Shtessel, C. Edwards, L. Fridman, and A. Levant, *Sliding Mode Control and Observation*, vol. 10. New York, NY, USA: Springer, 2014.

MIRZOBEK MALIKOV received the B.Sc. degree in mechanical engineering from Politecnico di Torino, Italy, in 2021. He is currently pursuing the M.Sc. degree in aerospace engineering with Gyeongsang National University, Republic of Korea. His research interest includes distributed control of multiple unmanned aerial vehicles.

VLADIMIR SHIN received the B.Sc. and M.Sc. degrees in applied mathematics from the Moscow State Aviation Institute, Moscow, Russia, in 1977 and 1979, respectively, and the Ph.D. degree in mathematics from the Russian Academy of Sciences, Moscow, in 1985. From 1984 to 1999, he was the Head of the Statistical Methods Laboratory, Institute of Informatics Problems, Russian Academy of Sciences. From 2003 to 2011, he was an Associate Professor with the School of Mechatronics, Gwangju Institute of Science and Technology, Gwangju, South Korea. From 2011 to 2021, he was a Professor with the Department of Information and Statistics, Gyeongsang National University, Jinju, South Korea, where he is currently a Senior Researcher. In 2021, he has retired. His research interests include estimation, filtering, tracking, and data fusion.

YOONSOO KIM (Member, IEEE) received the B.Eng. degree in aerospace engineering from Inha University, Republic of Korea, in 1999, the M.Sc. degree in aerospace engineering from the University of Minnesota, USA, in 2001, and the Ph.D. degree in aerospace engineering from the University of Washington, USA, in 2004. He was a Postdoctoral Researcher and a Senior Lecturer with the University of Leicester, U.K., from 2004 to 2007, and the University of Stellenbosch, Stellenbosch, South Africa, from 2007 to 2011, respectively. Since 2011, he has been a Faculty Member with the Department of Aerospace and Software Engineering, Gyeongsang National University, Republic of Korea, where he is currently a Professor. His research interest includes distributed control of networked dynamical systems.